Chapter 7
SiC Nanostructured Films

Silicon carbide films have been intensively investigated concerning their fabrications and properties. In general, the thickness of the fabricated silicon carbide films can range from many micrometers to many nanometers. In this chapter, however, we shall focus on the nanostructured SiC films including the films with thickness on the nanoscale and the films comprising SiC nanocrystals. We shall summarize the fabrication, structures, and properties of these nanostructured SiC films.

7.1 Synthesis by Chemical Vapor Deposition

Chemical vapor deposition is an important method for the preparation of the silicon carbide films. Internal stress in 3C-SiC epilayers grown on Si substrates by chemical vapor deposition using SiH_4–C_3H_8–H_2 as starting materials at 1,350 °C have been investigated by Raman scattering [1]. Raman scattering from the 3C-SiC epitaxial layers grown on Si(001) and Si(111) substrates shows that the LO phonon frequencies shift to the lower frequency side compared with stress-free 3C-SiC films. The frequency shift gives an estimate of the tensile stress of the 3C-SiC epilayer on Si(001) to be 5.4×10^9 dyn/cm^2. The stress difference between the 3C-SiC films on Si(001) and on Si(111) is smaller than that expected from the elastic deformation theory. A set of formulas have been derived [2, 3] to describe the Raman shifts of diamond and zinc-blende semiconductors under axial stress. The Raman shifts under hydrostatic pressure and uniaxial and biaxial stresses only act as special cases of the general formulas. Raman scattering measurements from a series of chemical vapor-deposited 3C-SiC films on (100) Si with thickness between 60 nm and 17 μm (Fig. 7.1) show that the Raman spectra in samples with SiC thickness greater than 4 μm exhibit a sharp and strong feature that obeys the selection rule for the 3C-SiC LO(Γ) phonon line. The stresses in 3C-SiC extracted

J. Fan and P.K. Chu, *Silicon Carbide Nanostructures*,
Engineering Materials and Processes, DOI 10.1007/978-3-319-08726-9_7

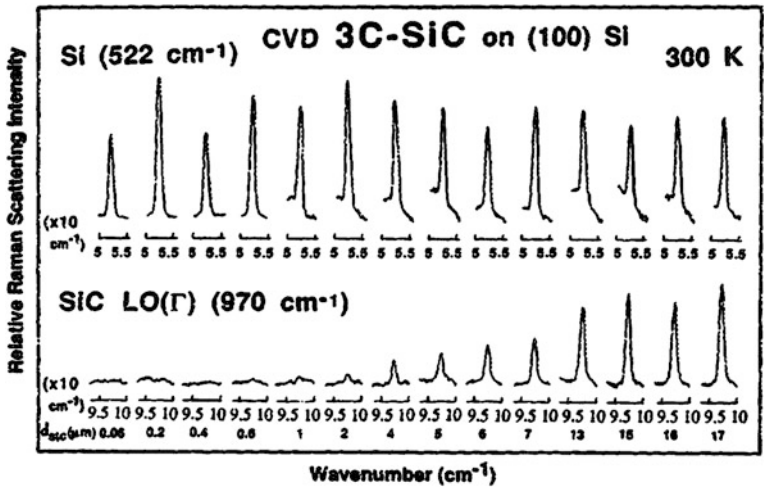

Fig. 7.1 Raman spectra of 14 chemical vapor-deposited 3C-SiC/Si samples with the SiC film thickness varying from 60 nm to 17 μm. Reprinted with permission from [3]. Copyright 1988, AIP Publishing LLC

from these data are between 0.3 and 1.1 GPa. 3C-SiC and Si have a large lattice mismatch of 20 %, but the difference in Raman shift between 3C-SiC/Si and free 3C-SiC films is smaller than 2 cm^{-1}, corresponding to strains of 0.1–0.2 %. The Raman signals from the SiC film and the Si substrate exhibit identical polarization behavior confirming their same crystalline orientations. The 3C-SiC LO(Γ) phonon signal shows an enhancement by a factor of 2 or 3 after removal of the Si substrate owing to multiple reflections in free 3C-SiC films.

Photoluminescence at 4.2 K in as-grown and ion-implanted 3C-SiC films grown by chemical vapor deposition on Si(100) substrates have been investigated [4]. The *D*1- and *D*2-defect PL bands previously observed in ion-implanted Lely-grown SiC are observed in the as-grown un-implanted films (Fig. 7.2), and they possess higher defect concentration than the vapor transport Lely-grown 3C-SiC crystals. The ion implantation in the SiC films causes significant enhancement in the intensities of the *D*1- and *D*2-defect bands. Their intensities in both as-grown and ion-implanted films increase after annealing at temperature up to 1,600 °C and above this temperature, the intensity of the *D*2 zero-phonon line decreases sharply, suggesting possible lattice recovery which quenches this defect emission band. The intensity of the *D*1 emission band remains nearly constant after annealing at temperature above 1,600 °C and up to 1,800 °C. Similar to the Lely-grown SiC, the spectral details of these defects-related PL bands and their annealing behaviors in the SiC films are independent of the implanted-ion species.

The photoluminescence at 2 K in 26 3C-SiC films with thickness of 60 nm to 25 μm grown on (100) Si by chemical vapor deposition have been investigated [5]. The bound-exciton PL spectrum (Fig. 7.3a) for the 3C-SiC-free film comprises the nitrogen-bound-exciton zero-phonon line N_0 along with its (one, two, and three)

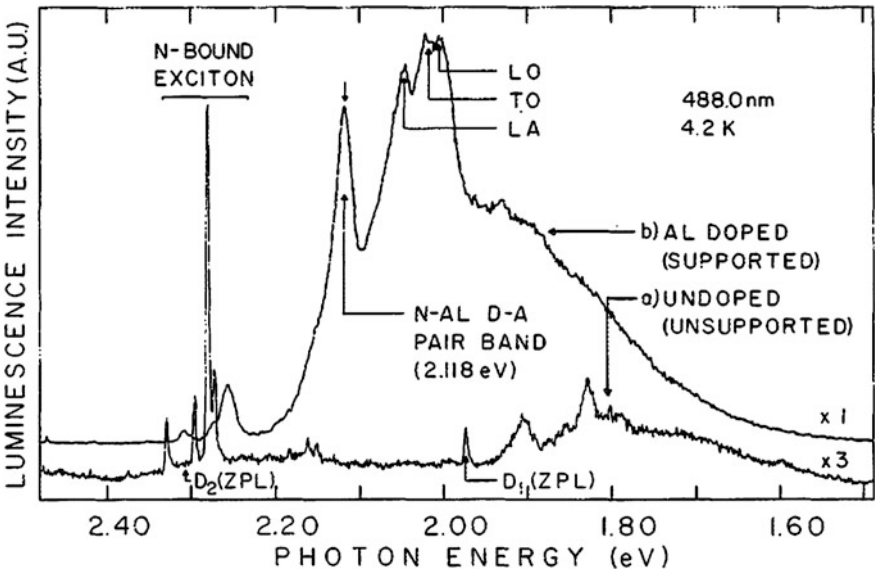

Fig. 7.2 PL spectra obtained from as-grown CVD 3C-SiC films. Spectrum **a** is from an undoped film that has been removed from its Si substrate. Spectrum **b** is from an Al-doped film on its Si substrate. Reprinted with permission from [4]. Copyright 1987, AIP Publishing LLC

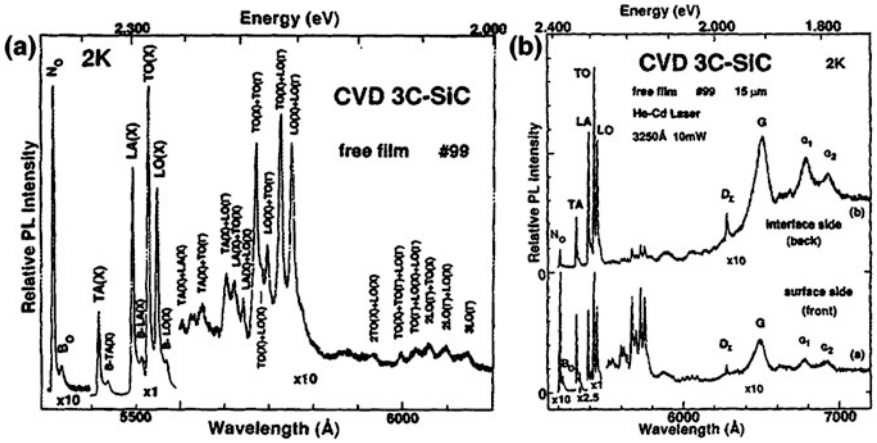

Fig. 7.3 **a** PL spectrum at 2 K showing the nitrogen-bound-exciton lines in a high-quality CVD free 3C-SiC film. **b** PL spectra at 2 K from both sides of a 15 μm CVD 3C-SiC film. Reprinted with permission from [5]. Copyright 1968, AIP Publishing LLC

phonon replicas. It also contains a *B*-series bound-exciton line (B_0) and its phonon replicas that are related to some unidentified impurity. The B_0 line shifts to lower energy side by 7 meV relative to the nitrogen-bound-exciton zero-phonon line.

The bound-exciton lines have a full width at half maximum (FWHM) smaller than 2 meV. The PL spectra (Fig. 7.3b) obtained from the front and back sides of a 3C-SiC film with thickness of 15 μm show much stronger bound-exciton lines in the near surface region than the near interface region. The D_I line is related to vacancies. The G band (near 1.90–1.92 eV) and its phonon replicas G_1 and G_2 bands as well as a background (below 1.95 eV) are all stronger in the interface layer than in the surface layer. This G band is associated with dislocations and extended defects. The very thin SiC films exhibit another defect-related W band near 2.15 eV.

Hydrogenated nanocrystalline silicon carbide films deposited on Si or corning glass substrates have been prepared by chemical vapor deposition using a mixture of methane, silane, and hydrogen as source gases [6]. Their infrared absorption spectrum shows a 3C-SiC TO phonon absorption band at around 794 cm^{-1}. The Raman spectrum (Fig. 7.4a) consists of three main peaks at 785.3, 986.4, and 1,606.5 cm^{-1} and a weak shoulder peak at 1,390.2 cm^{-1}. The first two bands are assigned to TO and LO phonon modes of SiC, and the peaks at 1,606.5 and 1,390.2 cm^{-1} are attributed to disordered graphite. The sample has strong room temperature photoluminescence centered at around 2.64 eV under 351 nm excitation, but the PL shifts to 2.2 eV under 325 nm excitation [7]. Figure 7.4b shows the PL and absorption spectra of two samples [8] prepared under different source gas ratios, and the flow ratio of $H_2/SiH_4/CH_4$ is 100:10:3 for sample D and 100:5:1 for sample E. Their time-resolved PL spectra (Fig. 7.4c) can be fit by double-exponential function with two decay time constants of 166 and 772 ps for sample D and 246 and 974 ps for sample E, respectively. These values are at least two orders of magnitude smaller than that of the bound-exciton transitions in bulk 3C-

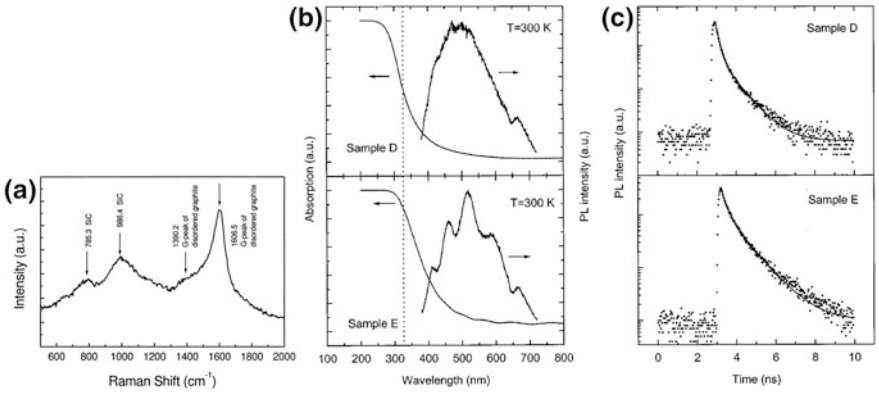

Fig. 7.4 **a** Raman spectrum of the chemical vapor-deposited SiC nanocrystalline film. Reprinted with permission from [6]. Copyright 2000, Elsevier. **b** Room temperature optical absorption and PL spectra (excited at 351 nm) and **c** time-resolved PL spectra (excited at 400 nm) of two chemical vapor-deposited SiC films. The *solid lines* show the double-exponential fit to the experimental data. Reprinted with permission from [8]. Copyright 2000, AIP Publishing LLC

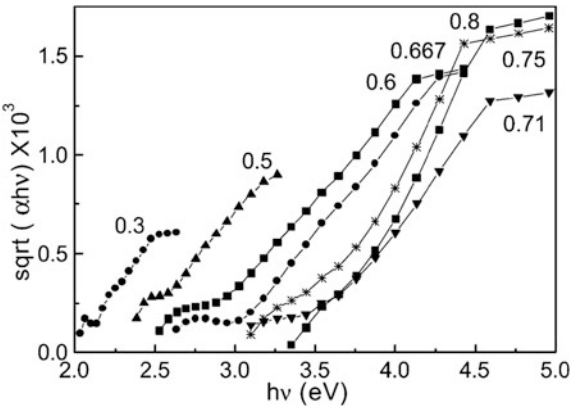

Fig. 7.5 Absorption (*square root* of absorbance) as a function of photon energy in a-SiC:H films that were prepared with different acetylene fractions. Reprinted with permission from [9]. Copyright 2001, Elsevier

SiC at low temperature. The double-exponential decay law suggests that multiple states are involved in the radiative recombination.

Hydrogenated amorphous silicon carbon films (a-SiC:H) prepared from a gas mixture of silane and acetylene by catalytic chemical vapor deposition [9] have optical bandgaps that increase with increasing acetylene to silane ratio (Fig. 7.5). The bandgap reaches 3.6 eV for a ratio over 0.8. The deposition rate decreases drastically with increasing acetylene fraction. These silicon carbide films have visible photoluminescence at room temperature. Nanocrystalline SiC films deposited by plasma-enhanced chemical vapor deposition at different gas flow ratios and at different deposition temperatures from 80 to 575 °C have been investigated [10]. Diethylsilane ($C_4H_{12}Si$) is the source gas, and different concentrations of hydrogen, argon, or helium are used as the dilution gases. The infrared spectral analysis indicates that the SiC nanocrystals embedded in the amorphous film begin to form at 300 °C. The crystallization degree increases with increasing temperature, and the crystalline fraction reaches 65 % at 575 °C. The hydrogen dilution gas results in the highest crystalline fraction. The high-resolution TEM measurement reveals the existence of the SiC nanocrystallites in the amorphous matrix with their sizes ranging from 2 to 10 nm (Fig. 7.6). The refractive index of the film increases roughly linearly with temperature. The optical bandgap of the film can be derived from the absorption spectrum using the following relation:

$$\alpha h\nu = B(h\nu - E_g)^2, \tag{7.1}$$

where α is the absorption coefficient, B is a constant, $h\nu$ is the photon energy, and E_g is the bandgap. Another characteristic value E_{04} is defined as the energy at which α equals 10^4 cm^{-1}. As shown in Fig. 7.6, both E_g and E_{04} increase monotonically with increasing deposition temperature. The bandgap value varies from 2.6 to 4.47 eV as the temperature increases from 80 to 575 °C, showing a large blueshift relative to the bulk value. The micro-Raman measurement reveals an average crystallite size of 4 nm. The TEM observation shows that the crystallite sizes are 2–10 nm and that only the concentration of the nanocrystallites in the

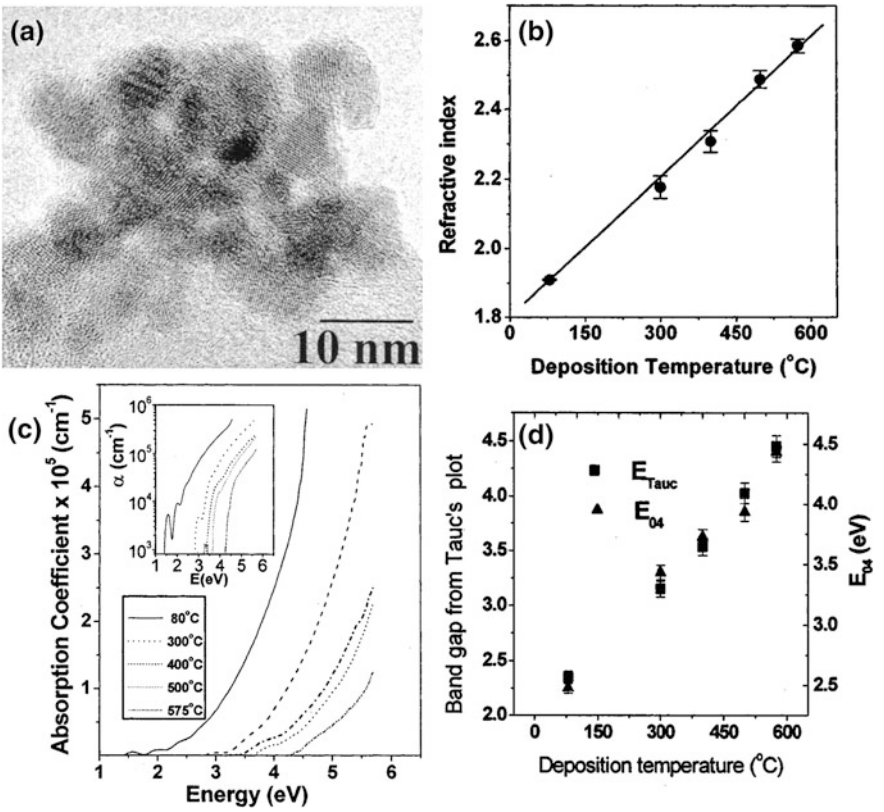

Fig. 7.6 **a** HRTEM image of the SiC film deposited with hydrogen dilution at 575 °C. **b** Refractive index versus deposition temperature. **c** Optical absorption spectra for the films deposited at different temperatures. The *inset* shows the same spectra in logarithmic scale. **d** Bandgap E_g and E_{04} as a function of deposition temperature. Reprinted with permission from [10]. Copyright 2003, AIP Publishing LLC

amorphous matrix increases with deposition temperature, whereas their sizes do not increase significantly with deposition temperature. Considering that the bandgap value is determined by both the amorphous SiC and the SiC nanocrystallites, hence the origin of large bandgap values is ascribed to the presence of nanocrystallites in the films.

Nanocrystalline silicon carbide films deposited on molybdenum substrates by thermal plasma chemical vapor deposition at substrate temperature of 750–1,250 °C [11] are mainly composed of β-SiC nanocrystallites. Characterization of the films by use of nanoindentation shows that their average grain size, crystalline fraction in the film, and film hardness all increase with increasing substrate temperature (Fig. 7.7). The average grain sizes are between 10 and 20 nm, the crystalline fraction is 80–85 %, and the film hardness is about 50 GPa in the film obtained with substrate temperature above 1,200 °C.

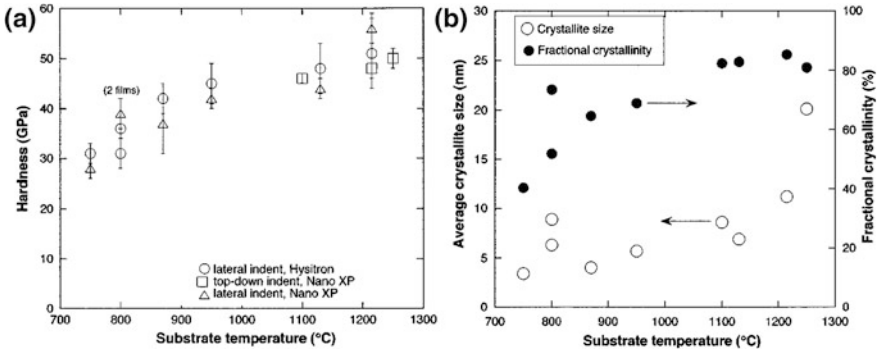

Fig. 7.7 **a** Film hardness as a function of substrate temperature during deposition of SiC film measured by nanoindenter. **b** Average crystallite size and crystalline fraction as a function of substrate temperature. Reprinted with permission from [11]. Copyright 2005, AIP Publishing LLC

Undoped and *n*- and *p*-type hydrogenated nanocrystalline 3C-SiC films have been deposited on glass and silicon substrates at substrate temperature of 300 °C by hot-wire chemical vapor deposition [12]. Monomethylsilane and hydrogen are the source gases for deposition of undoped films. Phosphine and hexamethyldisilazane are phosphorous and nitrogen sources for *n*-type doping, and dimethylaluminumhydride is aluminum source for *p*-type doping. Figure 7.8 shows the cross-sectional TEM images of the undoped films deposited at different H_2/monomethylsilane ratios, and the corresponding ring electron diffraction pattern corresponds to the crystalline phases of 3C-SiC. The XRD analysis indicates that the average grain size in the film increases from 6.4 to 16.6 nm with increasing deposition temperature. The grain size affects the dark conductivity and the dielectric functions of the films. The former increases from 5.8×10^{-11} to 6.2×10^{-6} S/cm as the grain size increases from 6.4 to 16.6 nm. The dark conductivities are 5.32 and 7.67×10^{-4} S/cm for the *n*- and *p*-type films, respectively. The absorption data reveal that *p*-type doping significantly affects absorption coefficients above the bandgap of the doped film, whereas the absorption coefficients below the bandgap of the *n*-type film are affected by free carrier absorption and localized states within the bandgap.

Silicon carbide films with different carbon concentrations have been synthesized by inductively coupled plasma chemical vapor deposition using a $SiH_4/CH_4/H_2$ gas mixture at a substrate temperature of 500 °C [13]. The film obtained with carbon concentration of 49 at% is composed of nanocrystalline cubic silicon carbide without any phase of silicon, graphite, or diamond crystallites (Fig. 7.9). The average size of SiC crystallites is about 6 nm. Polycrystalline silicon and amorphous silicon carbide coexist in the films obtained with lower carbon concentrations, and amorphous carbon and silicon carbide coexist in the films obtained with higher carbon concentrations.

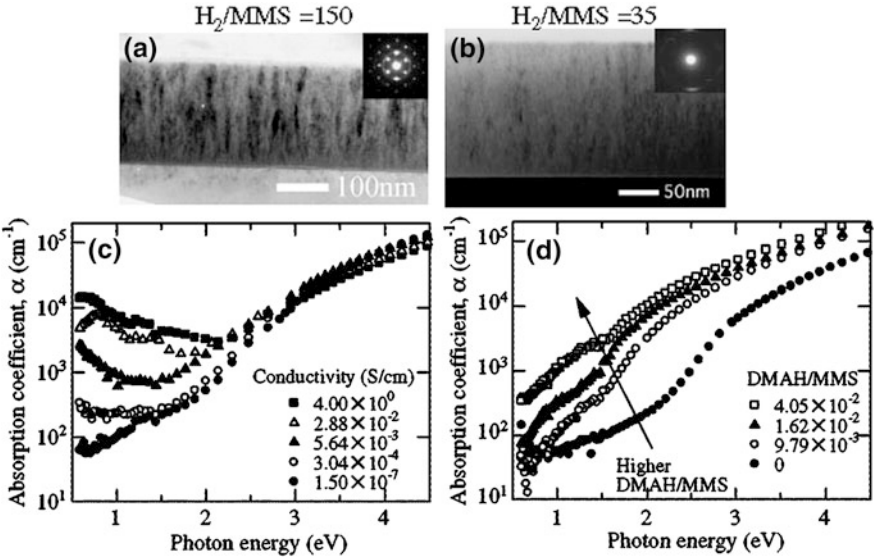

Fig. 7.8 **a**, **b** Cross-sectional TEM images of hydrogenated nanocrystalline 3C-SiC films deposited at different H_2/monomethylsilane ratios. **c** Absorption spectra of *n*-type SiC films with different dark conductivities. **d** Absorption spectra of *p*-type SiC films deposited at different dimethylaluminumhydride/monomethylsilane ratios. Reprinted with permission from [12]. Copyright 2007, Japanese Society of Applied Physics

Nanocrystalline SiC film has been deposited by helicon wave plasma-enhanced chemical vapor deposition on corning glass and single-crystal silicon substrates using a mixture of H_2, SiH_4, and CH_4 gases [14]. HRTEM observation (Fig. 7.10) reveals that the film comprises many 3C-SiC nanocrystals embedded in the amorphous SiC matrix with an average size of 3.96 nm. The SiC film shows photoluminescence with peak wavelength ranging from 475 to 545 nm as the excitation wavelength increases from 360 to 500 nm. This shifting emission implies that the photoluminescence may be governed by quantum confinement effect. The time-resolved photoluminescence shows an average lifetime on the order of nanosecond.

7.2 Fabrication by Ions Implantation

Ions implantation in combination with annealing is another widely used method for fabricating SiC films containing SiC nanocrystals. The SiC microcrystallites in Si single crystals have been fabricated by carbon ion implantation at fluence of $10^{17}/cm^2$ followed by annealing [15]. Infrared absorption examination reveals a broad absorption band centered at 700–725 cm^{-1} (Fig. 7.11) in as-implanted

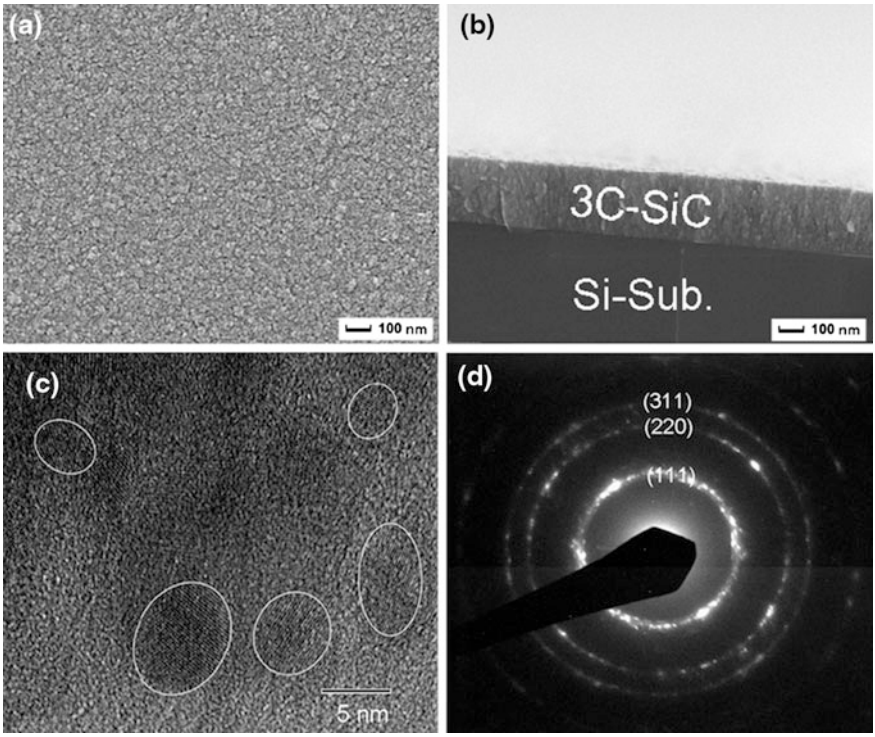

Fig. 7.9 **a**, **b** Surface morphology and fracture cross section of SiC film with carbon concentration of 49 at%. **c** HRTEM image and **d** electron diffraction pattern of the same SiC film. Reprinted with permission from [13]. Copyright 2007, IOP Publishing

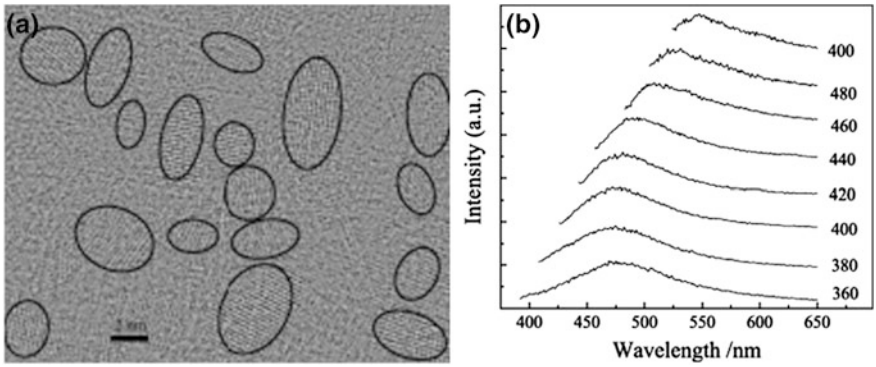

Fig. 7.10 **a** HRTEM image of the SiC film and **b** its PL spectra excited at different wavelengths. Reprinted with permission from [14]. Copyright 2011, Elsevier

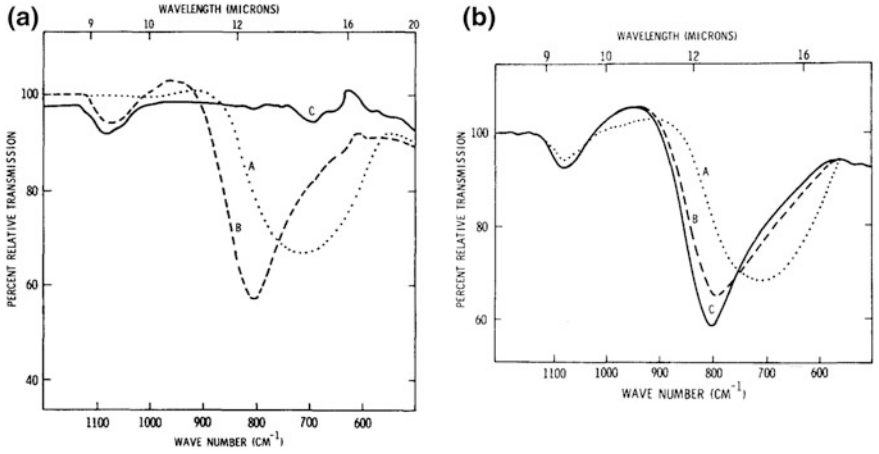

Fig. 7.11 **a** Infrared transmission spectra of (*A*) Si wafer implanted by 10^{17} carbon atoms/cm^2 before annealing; (*B*) same sample after annealing at 1,000 °C for 20 min; (*C*) un-implanted Si annealed at 1,000 °C for 20 min. All spectra are taken with matched un-implanted unannealed Si as the reference sample. **b** Infrared transmission spectra of a Si wafer implanted by 10^{17} carbon atoms/cm^2 followed by annealing for 20 min at (*A*) 800 and 825 °C, (*B*) 850 °C, and (*C*) 900 °C. Reprinted with permission from [15]. Copyright 1971, AIP Publishing LLC

sample, and it persists after annealing at temperature up to 825 °C. The band peak lies between the local mode of carbon in silicon (608 cm^{-1}) and the TO phonon mode of SiC (796 cm^{-1}) and is assigned to the former, and its broadening and shifting to higher frequencies is due to the high carbon concentration and the high disorder of the implanted layer. The SiC microcrystallites begin to form at temperature around 850 °C, as demonstrated by arising of the strong TO phonon absorption band of SiC at around 800 cm^{-1}. The annealing effect on the implanted film is completed by 875 °C, and there is no further change in the absorption band upon further anneal up to 1,000 °C. The annealed implanted and un-implanted samples all possess an absorption band at around 1,080 cm^{-1} attributed to the SiO_2 surface layer formed by annealing, and it vanishes after removal of the surface layer by HF etching.

The microcrystalline SiC in the Si matrix formed by carbon implantation has been investigated by TEM, X-ray diffraction, infrared absorption, Auger electron spectroscopy, Rutherford backscattering spectrometry, and nuclear reaction analysis [16]. A thick buried layer of β-SiC with a thickness of 300 nm forms after multiple implantations at 860 °C without further annealing. This buried layer consists of nanocrystalline SiC grains with an average size of 7 nm, and they show nearly perfect epitaxial relation with the Si matrix. The grains are only slightly misorientated by 3.5° and are significantly twinned on {111} planes.

The β-SiC in Si crystal matrix has been fabricated by carbon ions implantation into Si wafers for ion energy of 50 keV and dose of 10^{17} cm^{-2} followed by annealing in nitrogen at 950 °C [17]. The TEM observation reveals the formation

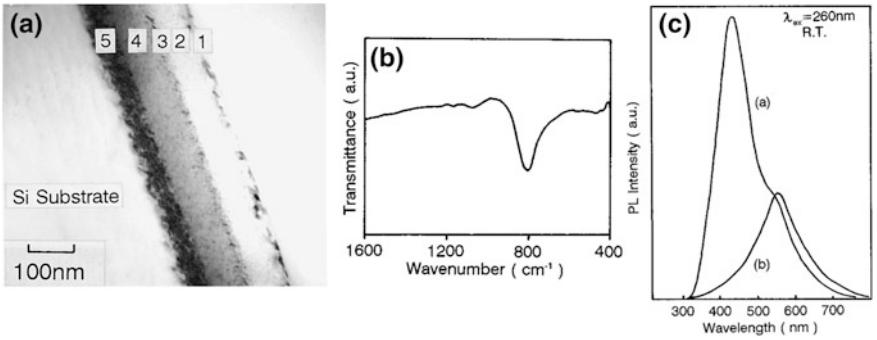

Fig. 7.12 **a** TEM image of the C^+-implanted Si crystal after annealing in N_2 at 950 °C. Regions 1–5 are successively upper damaged Si layer, β-SiC precipitate, closure boundary, β-SiC precipitate, and lower damaged Si layer. **b** FTIR spectrum of this sample. **c** PL spectra of annealed C^+-implanted sample [curve (a)] and reference sample without implantation [curve (b)]. Both samples are anodized in HF-ethanol solution at 40 mA/cm^2. Reprinted with permission from [17]. Copyright 1995, AIP Publishing LLC

of a layer of polycrystalline β-SiC beneath the sample surface (Fig. 7.12), and the electron diffraction pattern shows features in accordance with polycrystalline β-SiC. The infrared spectrum has a strong absorption band at around 800 cm^{-1} that is assigned to the TO phonon mode of β-SiC. The porous SiC is achieved by etching the implanted and annealed sample in HF-ethanol (2:1 by volume) solution at a current density of 40 mA/cm^2 with assistance of UV-light illumination. The resultant porous sample has photoluminescence with two peaks at around 445 nm (2.79 eV) and 560 nm under 260-nm excitation. The former peak photon energy is higher than the bandgap of bulk β-SiC (2.2 eV), and this band may stem from the interband transition in the β-SiC nanocrystallites. The latter emission band is assigned to the porous Si. The distribution of the β-SiC nanocrystallites in the Si matrix has been investigated [18] for samples achieved by carbon ion implantation into Si wafers at an energy 50 keV and a dose 5×10^{17} cm^{-2} at 600 °C followed by anneal in nitrogen at 1,100 °C. The cross-sectional TEM image (Fig. 7.13) of the as-implanted sample reveals three layers from the implanted surface down to the substrate, they are the upper damaged Si layer A (85 nm thick), the amorphous layer B (70 nm thick), and the lower damaged Si layer C (50 nm thick). After annealing, three layers have distinct concentrations of SiC nanocrystals due to distribution of implanted ions; the concentration is low in layers A and C and reaches a maximum at the B/C interface. The embedded β-SiC crystallites have size of 2–8 nm.

The β-SiC nanocrystals have been synthesized by carbon implantation into Si crystals at 35 keV with various doses followed by annealing at 1,200 °C in argon atmosphere and subsequent thermal oxidation at 1,050 °C [19]. The infrared spectrum (Fig. 7.14) shows two strong absorption peaks, one shifts from 820 to 795 cm^{-1} as implantation dose increases from 1.2×10^{16} to 3.2×10^{17} cm^{-1},

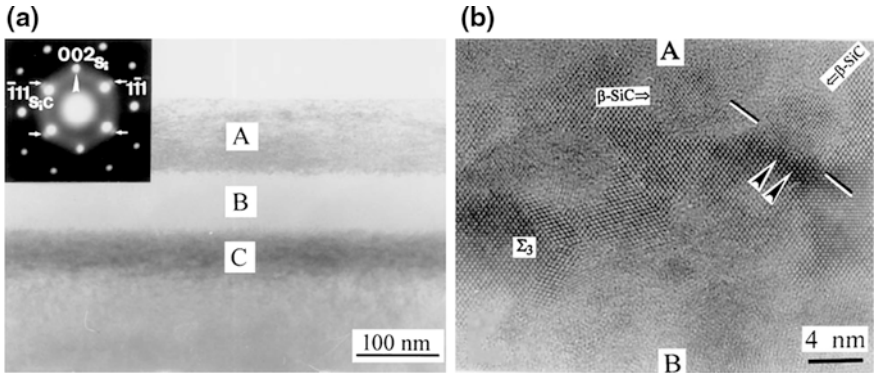

Fig. 7.13 **a** Cross-sectional TEM image showing three layers on the surface of carbon-implanted Si crystal without annealing. The *inset* is the electron diffraction pattern of this layered structure showing spots from Si matrix and β-SiC particles and a halo from the amorphous phase. **b** HRTEM image of the A/B interface in the annealed sample showing epitaxial growth and amorphous interface between Si and β-SiC nanocrystals. Reprinted with permission from [18]. Copyright 1997, Cambridge University Press

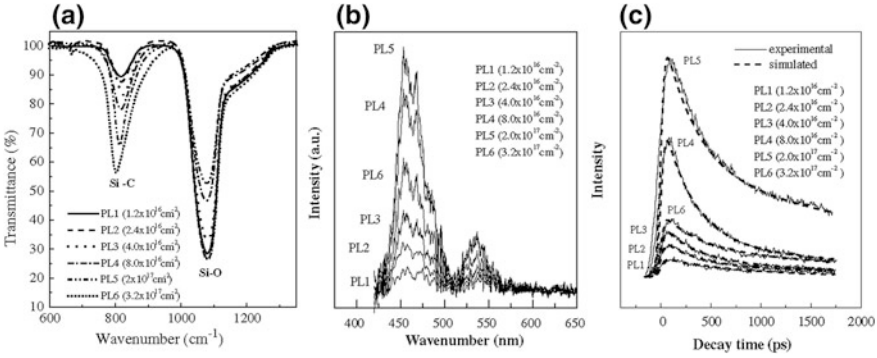

Fig. 7.14 **a** FTIR spectra of the carbon ion-implanted single-crystal Si at 35 keV with various doses. The samples are annealed at 1,200 °C in argon atmosphere and oxidized at 1,050 °C. **b** PL spectra of the samples excited at 300 nm at room temperature. **c** Time-resolved PL spectra of the samples. Reprinted with permission from [19]. Copyright 2003, Elsevier

and it is assigned to the TO phonon mode of β-SiC, another at around 1,080 cm^{-1} is assigned to the Si–O–Si vibration of the SiO_2 film formed on the sample surface. The sample has photoluminescence with two bands at around 460 and 535 nm under 300-nm excitation. Time-resolved photoluminescence spectrum of the sample comprises two decay components with lifetimes of around 3 and 0.35 ns, respectively.

The embedded SiC nanocrystallites can also be prepared by ion implantation into SiO_2 films instead of Si films. The quasi-white photoluminescence has been

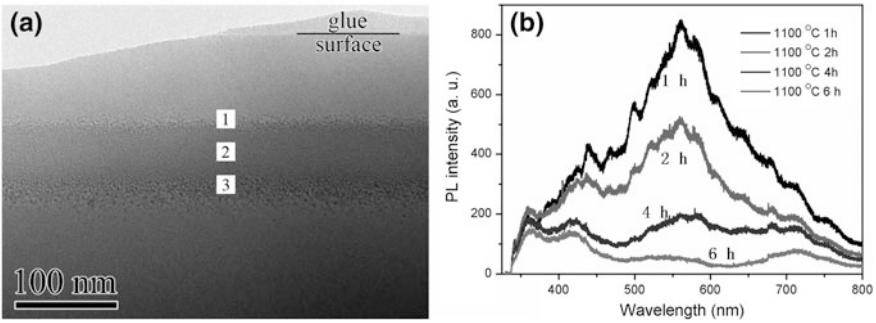

Fig. 7.15 **a** Cross-sectional TEM image of the Si^+/C^+ co-implanted silica wafer after annealing at 1,100 °C showing three layers. There are many Si and SiC nanocrystals in regions 1 and 3. **b** PL spectra of the Si^+/C^+ co-implanted silica wafer before annealing and after annealing at different temperatures. Reprinted with permission from [20]. Copyright 2012, AIP Publishing LLC

observed from the silica wafer implanted by Si^+ and C^+ ions or only by C^+ ions followed by thermal annealing in argon atmosphere [20]. The TEM measurement (Fig. 7.15a) reveals that the annealed Si^+/C^+ co-implanted silica wafer has three distinct layers beneath the surface. There are many Si and SiC nanocrystals in regions 1 and 3. The sample has wide photoluminescence band (Fig. 7.15b) in the range of 350–800 nm with maximum at around 550 nm. This quasi-white light emission arises from the graphitic carbon clusters as well as the Si and SiC nanocrystals.

Diamond is also employed as the implantation substrate for the synthesis of the embedded SiC crystallites. The natural IIa diamond has been used as the substrate to produce SiC by implantation of 90 keV N^+ at a dose of $1 \times 10^{15}/cm^2$ followed by implantation of 150 keV Si^+ at a dose of $3 \times 10^{17}/cm^2$ at 900 °C [21]. Cross-sectional transmission electron microscopy (Fig. 7.16) reveals a 70-nm-thick damaged diamond layer (zone A) and a 150-nm-thick buried layer (zone B) in which crystalline 3C-SiC domains are in perfect epitaxial relation to the weakly damaged diamond matrix. No amorphous or graphitic domains are present in the implanted layer owing to the high implantation temperature. There is an array of ordered misfit dislocations at the 3C-SiC/diamond interface. The Raman spectrum comprises a diamond signal at 1,332 cm^{-1} and a weak peak at 797 cm^{-1} that is characteristic of 3C-SiC TO phonon mode. The infrared spectroscopy reveals 3C-SiC TO phonon absorption at around 796 cm^{-1}. The implantation temperature affects the structural properties of the Si-implanted diamond [22]. Implantation with high Si fluence severely damages the diamond matrix and the formed SiC crystallites. Raising the implantation temperature from 900 to 1,000 °C diminishes damage and increases the SiC crystallite concentration, size, and epitaxial alignment. Further increase of the implantation temperature does not improve the quality of the SiC-rich layer, and in this case the damaged diamond transforms into graphite.

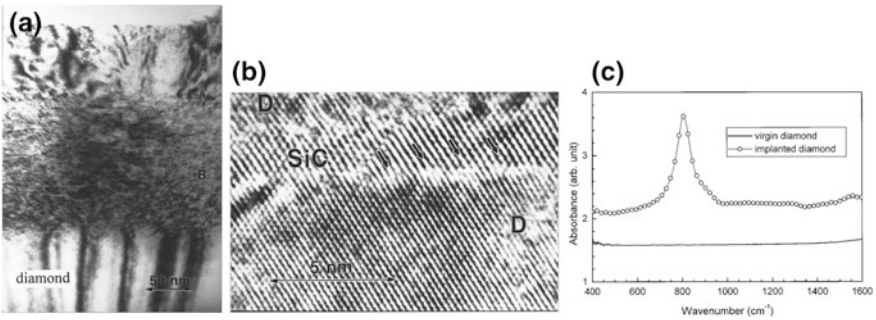

Fig. 7.16 **a** Cross-sectional TEM image of diamond doped successively by N^+ and Si^+. Zone *A* (*upper layer*) is the damaged crystalline diamond, and Zone *B* (*middle layer*) is where the implanted Si atoms lie. **b** High-resolution micrograph of a 3C-SiC domain embedded in the diamond matrix of Zone *B*. Letter D denotes diamond, and the *arrows* indicate the misfit dislocations. **c** Infrared absorption spectra of pristine and implanted diamond. Reprinted with permission from [21]. Copyright 2000, AIP Publishing LLC

7.3 Fabrication by Sputtering

Sputtering is another common method to prepare silicon carbide nanostructured films. Silicon carbide thin films have been deposited by reactive magnetron co-sputtering of silicon and carbon on silicon or quartz substrates in pure hydrogen plasma at substrate temperature of 100–600 °C [23]. Infrared absorption and TEM measurements (Fig. 7.17) indicate that the crystalline SiC begins to form at a substrate temperature of 300 °C. The crystalline fraction increases with substrate temperature as demonstrated by the increase in intensity of the infrared absorption at 800 cm^{-1} that is assigned to the stretching vibration of Si–C bonds. The weaker absorptions at about 900 and 1,000 cm^{-1} are separately assigned to the $Si–H_2$ bending and C–H wagging modes, and their respective stretching modes are present at 2,100 and 2,900 cm^{-1}. The electron diffraction ring stemming from the β-SiC (111) lattice planes becomes more clear with increasing substrate temperature above 300 °C, confirming the improvement of crystalline fraction. The refractive index of the layers increases from 1.9 to 2.4, and the room temperature dark conductivity increases by six orders of magnitude as the substrate temperature increases from 100 to 600 °C. High-resolution transmission electron microscopy reveals the formation of randomly oriented β-SiC nanocrystals with an average size of a few nanometers for substrate temperature over 400 °C [24].

The deposition temperature influences the growth of sputtered nanocrystalline SiC [25]. The sputtered film contains SiC nanocrystals with an average size of about 5 nm (Fig. 7.18a), and the number density increases with increasing deposition temperature. The sputtered film contains also the cubic SiC crystallites possessing 6H-SiC faults. The optical transmission measurement performed on the sputtered SiC layers gives their static refractive index and pseudo–bandgap $E_{5.4}$, which is the energy corresponding to the absorption coefficient of 5×10^4 cm^{-1},

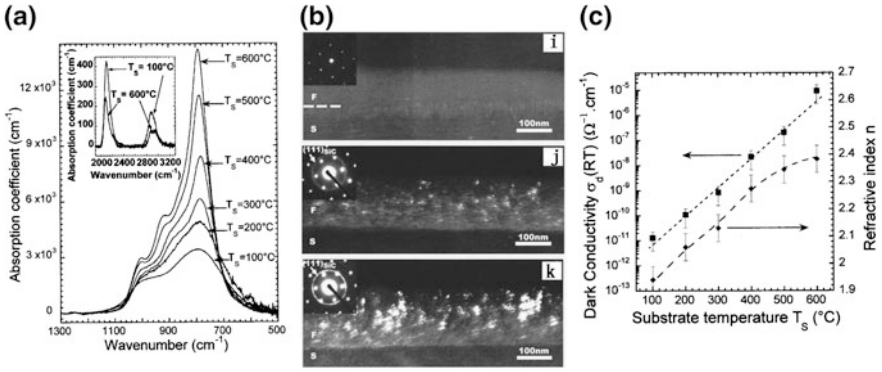

Fig. 7.17 **a** Infrared absorption spectra in the 500–1,300 cm^{-1} region for the SiC layers obtained by co-sputtering of silicon and carbon at different substrate temperatures. The *inset* shows two typical spectra in the 1,900–3,300 cm^{-1} range. **b** Cross-sectional TEM images and corresponding electron diffraction patterns of the SiC films grown at (*i*) 200 °C, (*j*) 300 °C, and (*k*) 600 °C. **c** Refractive index and room temperature dark conductivity as a function of substrate temperature. Reprinted with permission from [23]. Copyright 2000, AIP Publishing LLC

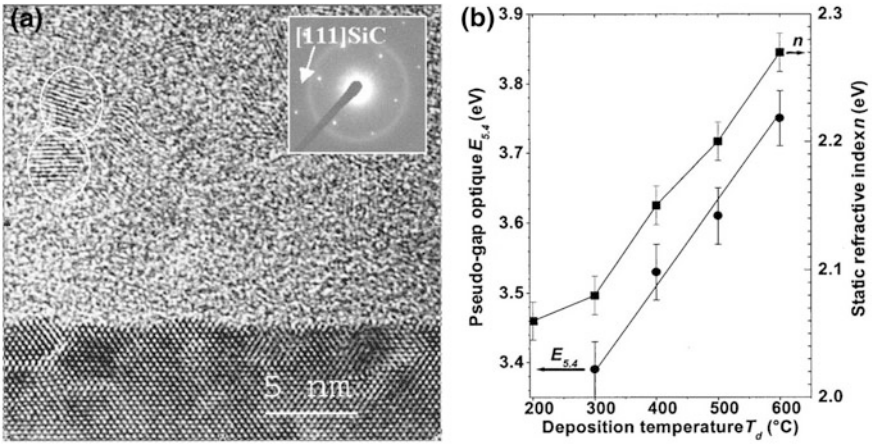

Fig. 7.18 **a** Cross-sectional TEM image for SiC film grown by co-sputtering of silicon and carbon at deposition temperature of 300 °C. The *inset* shows corresponding selected area electron diffraction pattern. **b** Pseudogap $E_{5.4}$ obtained from absorption spectra and static refractive index as a function of deposition temperature. The *solid lines* are the guide for the eyes. Reprinted with permission from [25]. Copyright 2005, AIP Publishing LLC

and both quantities increase with deposition temperature (Fig. 7.18b). The slight increase of the pseudo–bandgap results from variation of the Si/C ratio and decrease of the hydrogen content in the SiC film with increasing deposition temperature.

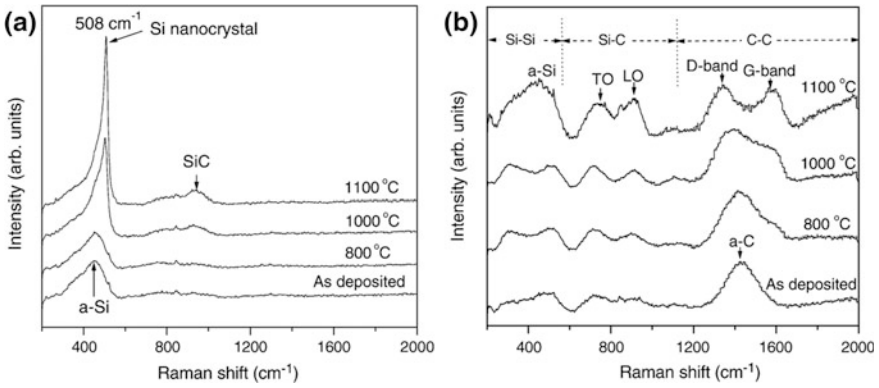

Fig. 7.19 Raman spectra of the Si and C co-sputtered films obtained with C/Si ratios of 0.33 (**a**) and 0.71 (**b**). The major peaks and annealing temperatures are indicated. Reprinted with permission from [27]. Copyright 2008, Elsevier

The Si nanocrystals may coexist with the SiC nanocrystals in the Si and C co-sputtered films. The three-layer amorphous Si/C/amorphous Si films containing nanocrystalline SiC have been prepared by ion-beaming sputtering of silicon and carbon on the Si substrates and subsequent annealing at 750 °C in vacuum [26]. The SiC nanocrystals with diameters of 20–120 nm are present on the top and at the bottom of the three-layer film. The two Si/C interfaces comprise SiC nanocrystals and Si nanocrystals with sizes below 5 nm, and these nanocrystals are embedded in an amorphous SiC matrix. The three-layer film has photoluminescence with a single peak centered at around 480 nm under 325-nm excitation. $Si_{1-x}C_x$ films with varying carbon-to-silicon ratios have been fabricated by magnetron co-sputtering of C and Si targets [27]. The composition of the films changes with varying ratio of two targets. The as-sputtered films have been annealed at various temperatures from 800 to 1,100 °C in nitrogen atmosphere. The infrared absorption spectrum contains a Si–C stretching peak that shifts from 737 to 800 cm^{-1} as annealing temperature increases. Raman scattering (Fig. 7.19), X-ray diffraction, and transmission electron microscopy reveal that the dominant nanocrystals in the sputtered film change from Si to SiC in the films annealed at 1,100 °C when the C/Si atomic ratio increases from 0.33 to 1.02. Co-sputtering of silicon and carbon targets on silica or silicon substrates followed by annealing can also yield silicon nanocrystals embedded in an amorphous SiC matrix [28].

The β-SiC nanocrystals can be fabricated by relaxation of $Si_{1-y}C_y$ ($0.005 > y > 0.05$) random alloys grown epitaxially on Si [29]. At temperatures over 900 °C, the C atoms that are located in substitutional sites at lower temperatures will precipitate out of the lattice, leading to the formation of β-SiC nanocrystals with the same lattice orientation as that of the mother Si lattice. The nanocrystals have uniform diameters, and they are between 2 and 4 nm for $y = 0.005$ $Si_{1-y}C_y$ material. The β-SiC materials with high surface area and porosity have been prepared by reaction between mesoporous carbon and gaseous

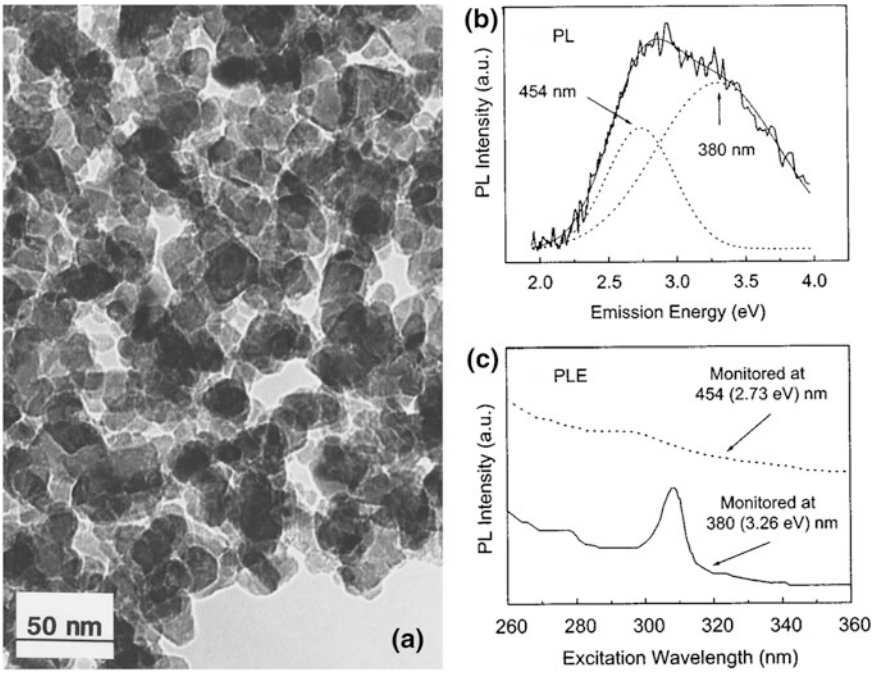

Fig. 7.20 **a** TEM image of a SiC film obtained by annealing C_{60} films on Si substrate at 900 °C. Unreacted carbon in the grain bulk gives a darker color to some grains. Reprinted with permission from [31]. Copyright 1997, AIP Publishing LLC. **b** PL spectrum of annealed C_{60}-coated porous Si. *Dotted lines* are the double-Gaussian fit of the curve. **c** PL excitation spectra of the sample. Reprinted with permission from [32]. Copyright 2000, AIP Publishing LLC

silicon coming from sublimation of the Si powder at temperature 1,200–1,300 °C [30]. The synthesized SiC sample has mesoporosity dimension of 5–40 nm.

Deposition and annealing of the 200-nm-thick C_{60} film on (100) silicon substrate can give rise to silicon carbide films [31]. The reaction between C_{60} and silicon starts at the interface and continues by silicon diffusion. Silicon diffusion and SiC formation require annealing at 800 °C for $t > 100$ min and at 900 °C for $t > 25$ min. The synthesized stoichiometric SiC film is uniform with a grain size of 20–40 nm (Fig. 7.20a). SiC nanocrystals can also be prepared by annealing C_{60}-covered porous Si [32]. X-ray diffraction reveals the existence of β-SiC particles along with Si, SiO_2, and graphite. The annealed sample has photoluminescence (Fig. 7.20b) with an asymmetric band, and the double-Gaussian fit of the curve gives two peaks at 380 nm (3.26 eV) and 454 nm (2.73 eV). The 380-nm band has an excitation peak at 308 nm (Fig. 7.20c), and this luminescence is suggested to arise from oxygen-vacancy defect in the SiO_2 matrix; the 454-nm band is related to the β-SiC particles.

The high-temperature reaction between Si wafer and carbon source material has been employed to synthesize the nanocrystalline SiC films [33]. The SiC

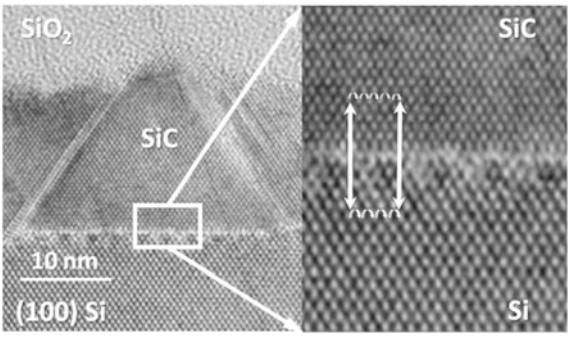

Fig. 7.21 HRTEM image of a SiC nanocrystal grown on Si (100) surface by annealing at 1,100 °C in 5 % CO. The nanocrystals are located at the SiO_2/Si interface. The SiC/Si interface is void-free and abrupt. Reprinted with permission from [33]. Copyright 2012, Elsevier

nanocrystals have been epitaxially and void-free grown on single-crystal Si substrates by reactive annealing process in CO at 1,100–1,190 °C. Crystal orientation shows influence on the nucleation density, size, and morphology of the nanocrystals. Irregular and large crystallites (63 nm) are prepared on the Si (111) surface for annealing in diluted CO (5 %). The SiC nanocrystals grown on the (100) surfaces are a few tens of nanometers in diameter (Fig. 7.21). Much smaller grains are prepared on the Si (110) planes. The substrate orientation affects only the morphology for annealing in pure CO.

Direct sputtering of SiC targets can produce the SiC nanocrystals. The SiC–SiO_2 composite film has been fabricated by co-sputtering of SiC and SiO_2 targets on the Si wafer [34]. The as-deposited sample experiences post-anneal at 400–1,200 °C. High-resolution TEM observation indicates that the as-deposited SiC–SiO_2 film is amorphous, but the SiC nanocrystals with diameters of about 5 nm are present in the sample annealed at 740 °C. The annealed SiC–SiO_2 composite film has photoluminescence at around 460 nm (2.7 eV) (Fig. 7.22). The luminescence intensity is strongly dependent on the annealing temperature, and it reaches a maximum at 950 °C. The infrared transmission measurement reveals two strong absorption bands at around 816 and 1,055 cm^{-1}: the former is the optical vibration mode of SiC, and the latter is attributed to the Si–O–Si vibration.

The β-SiC films have been fabricated on Si substrates by pulsed laser deposition using a polycrystalline SiC target [35]. High-resolution TEM observation (Fig. 7.23) reveals that the deposited film contains both β-SiC and Si nanocrystallites. The infrared spectrum has a strong absorption band at around 780 cm^{-1}, which is the TO phonon mode of β-SiC. Another shoulder peak at about 1,020 cm^{-1} is assigned to the Si–O–Si vibration. The film has photoluminescence with two adjacent peaks at 416 and 435 nm. The corresponding photoluminescence excitation spectrum contains a strong peak at 370 nm. The luminescence arises from the surface defect. The nanocrystalline SiC films comprising uniform-sized nanoislands have been prepared by plasma-assisted RF (radio frequency)

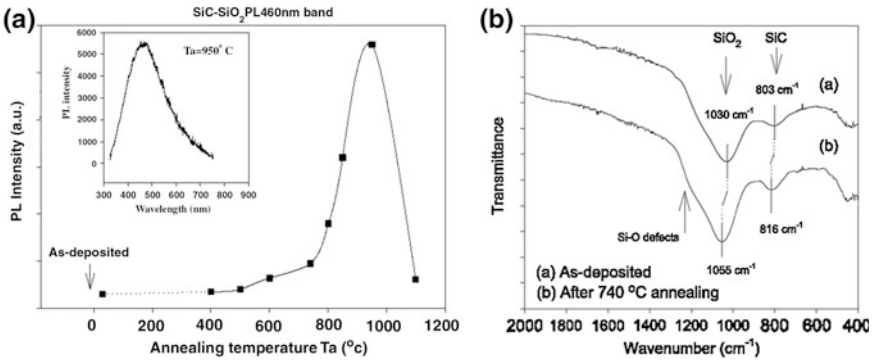

Fig. 7.22 **a** Intensity of PL at 460 nm in SiC-SiO_2 composite film under 325-nm excitation as a function of annealing temperature. The *inset* shows the PL spectrum of the SiC–SiO_2 film annealed at 950 °C. **b** FTIR spectra of the as-deposited and annealed SiC–SiO_2 composite film. Reprinted with permission from [34]. Copyright 2001, Elsevier

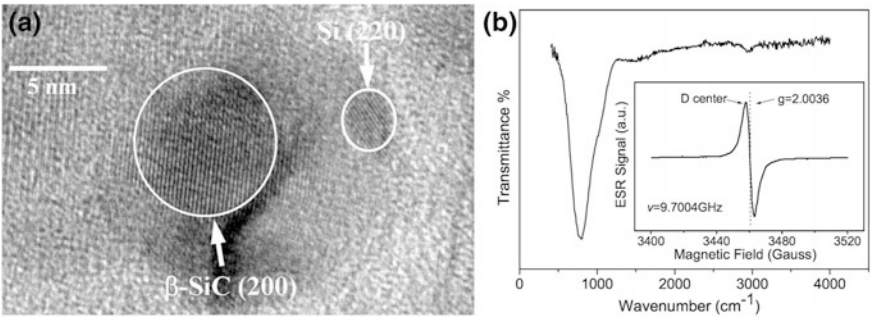

Fig. 7.23 **a** HRTEM image of the β-SiC film deposited on the (100) Si wafer showing Si and β-SiC nanocrystallites. **b** FTIR spectrum of the β-SiC film. The *inset* shows the electron paramagnetic resonance spectrum.Reprinted with permission from [35]. Copyright 2003, Elsevier. Reprinted with permission from [35]. Copyright 2003, Elsevier

magnetron sputtering deposition on the Si (100) surface using a SiC target [36]. The nanoislands have size of 20–35 nm and contain small (5 nm) nanocrystalline inclusions.

References

1. Mukaida H, Okumura H, Lee JH, Daimon H, Sakuma E, Misawa S, Endo K, Yoshida S (1987) Raman scattering of SiC: estimation of the internal stress in 3C-SiC on Si. J Appl Phys 62:254–257
2. Feng ZC, Choyke WJ, Powell JA (1988) Raman determination of layer stresses and strains for heterostructures and its application to the cubic SiC/Si system. J Appl Phys 64:6827–6835

3. Feng ZC, Mascarenhas AJ, Choyke WJ, Powell JA (1988) Raman scattering studies of chemical-vapor-deposited cubic SiC films of (100) Si. J Appl Phys 64:3176–3186
4. Freitas JA, Bishop SG, Edmond JA, Ryu J, Davis RF (1987) Photoluminescence spectroscopy of ion-implanted 3C-SiC grown by chemical vapor deposition. J Appl Phys 61:2011–2016
5. Choyke WJ, Feng ZC, Powell JA (1988) Low-temperature photoluminescence studies of chemical-vapor-deposition-grown 3C-SiC on Si. J Appl Phys 64:3163–3175
6. Yu MB, Rusli U, Yoon SF, Xu SJ, Chew K, Cui J, Ahn J, Zhang Q (2000) Hydrogenated nanocrystalline silicon carbide films synthesized by ECR-CVD and its intense visible photoluminescence at room temperature. Thin Solid Films 377–378:177–181
7. Yu MB, Rusli, Yoon SF, Chen ZM, Ahn J, Zhang Q, Chew K, Cui J (2000) Deposition of nanocrystalline cubic silicon carbide films using the hot-filament chemical-vapor-deposition method. J Appl Phys 87:8155–8158
8. Xu SJ, Yu MB, Rusli, Yoon SF, Che CM (2000) Time-resolved photoluminescence spectra of strong visible light-emitting SiC nanocrystalline films on Si deposited by electron-cyclotron-resonance chemical-vapor deposition. Appl Phys Lett 76:2550–2552
9. Kumbhar A, Patil SB, Kumar S, Lal R, Dusane RO (2001) Photoluminescent, wide-bandgap a-SiC: H alloy films deposited by Cat-CVD using acetylene. Thin Solid Films 395:244–248
10. Rajagopalan T, Wang X, Lahlouh B, Ramkumar C, Dutta P, Gangopadhyay S (2003) Low temperature deposition of nanocrystalline silicon carbide films by plasma enhanced chemical vapor deposition and their structural and optical characterization. J Appl Phys 94:5252–5260
11. Liao F, Girshick SL, Mook WM, Gerberich WW, Zachariah MR (2005) Superhard nanocrystalline silicon carbide films. Appl Phys Lett 86:171913
12. Miyajima S, Yamada A, Konagai M (2007) Characterization of undoped, n- and p-type hydrogenated nanocrystalline silicon carbide films deposited by hot-wire chemical vapor deposition at low temperatures. Jpn J Appl Phys 46:1415–1426
13. Cheng Q, Xu S, Long J, Huang S, Guo J (2007) Homogeneous nanocrystalline cubic silicon carbide films prepared by inductively coupled plasma chemical vapor deposition. Nanotechnology 18:465601
14. Yu W, Wang X, Geng C, Lve X, Lu W, Fu G (2011) Decay processes of photoluminescence in a nanocrystalline SiC thin film. Appl Surf Sci 258:1733–1737
15. Borders JA, Picraux ST, Beezhold W (1971) Formation of SiC in silicon by ion implantation. Appl Phys Lett 18:509–511
16. Martin P, Daudin B, Dupuy M, Ermolieff A, Olivier M, Papon AM, Rolland G (1990) High-temperature ion beam synthesis of cubic SiC. J Appl Phys 67:2908–2912
17. Liao L-S, Bao X-M, Yang Z-F, Min N-B (1995) Intense blue emission from porous β-SiC formed on C^+-implanted silicon. Appl Phys Lett 66:2382–2384
18. Gao YH, Zhang Z, Liao LS, Bao XM (1997) A high-resolution electron microscopy study of blue-light emitting β-SiC nanoparticles in C^+-implanted silicon. J Mater Res 12:1640–1645
19. Chen D, Liao ZM, Wang L, Wang HZ, Zhao F, Cheung WY, Wong SP (2003) Photoluminescence from β-SiC nanocrystals embedded in SiO_2 films prepared by ion implantation. Opt Mater 23:65–69
20. Zhou XD, Ren F, Xiao XH, Xu JX, Dai ZG, Cai GX, Jiang CZ (2012) Origin of white light luminescence from Si^+/C^+ sequentially implanted and annealed silica. J Appl Phys 111:084304
21. Heera V, Fontaine F, Skorupa W, Pécz B, Barna Á (2000) Ion-beam synthesis of epitaxial silicon carbide in nitrogen-implanted diamond. Appl Phys Lett 77:226–228
22. Weishart H, Eichhorn F, Heera V, Pécz B, Barna Á, Skorupa W (2005) High-fluence Si-implanted diamond: optimum implantation temperature for SiC formation. J Appl Phys 98:043503
23. Kerdiles S, Berthelot A, Gourbilleau F, Rizk R (2000) Low temperature deposition of nanocrystalline silicon carbide thin films. Appl Phys Lett 76:2373–2375

24. Kerdiles S, Rizk R, Gourbilleau F, Pérez-Rodríguez A, Garrido B, González-Varona O, Morante JR (2000) Low temperature direct growth of nanocrystalline silicon carbide films. Mater Sci Eng B 69–70:530–535
25. Colder H, Rizk R, Morales M, Marie P, Vicens J, Vickridge I (2005) Influence of substrate temperature on growth of nanocrystalline silicon carbide by reactive magnetron sputtering. J Appl Phys 98:024313
26. Chung CK, Chen TY, Lai CW (2011) Low-temperature formation of nanocrystalline SiC particles and composite from three-layer Si/C/Si film for the novel enhanced white photoluminescence. J Nanopart Res 13:4821–4828
27. Song D, Cho E-C, Cho Y-H, Conibeer G, Huang Y, Huang S, Green MA (2008) Evolution of Si (and SiC) nanocrystal precipitation in SiC matrix. Thin Solid Films 516:3824–3830
28. Chang G-R, Ma F, Ma D-Y, Xu K-W (2010) Multi-band silicon quantum dots embedded in an amorphous matrix of silicon carbide. Nanotechnology 21:465605
29. Powell AR, LeGoues FK, Iyer SS (1994) Formation of β-SiC nanocrystals by the relaxation of $Si_{1-y}Cy$ random alloy layers. Appl Phys Lett 64:324–326
30. Liu Z, Shen W, Bu W, Chen H, Hua Z, Zhang L, Li L, Shi J, Tan S (2005) Low-temperature formation of nanocrystalline β-SiC with high surface area and mesoporosity via reaction of mesoporous carbon and silicon powder. Micropor Mesopor Mat 82:137–145
31. Moro L, Paul A, Lorents DC, Malhotra R, Ruoff RS, Lazzeri P, Vanzetti L, Lui A, Subramoney S (1997) Silicon carbide formation by annealing C_{60} films on silicon. J Appl Phys 81:6141–6146
32. Wu XL, Siu GG, Stokes MJ, Fan DL, Gu Y, Bao XM (2000) Blue-emitting β-SiC fabricated by annealing C_{60} coupled on porous silicon. Appl Phys Lett 77:1292–1294
33. Battistig G (2012) Orientation dependent growth of SiC nanocrystals at the SiO_2/Si interface. Thin Solid Films 520:1973–1977
34. Guo YP, Zheng JC, Wee ATS, Huan CHA, Li K, Pan JS, Feng ZC, Chua SJ (2001) Photoluminescence studies of SiC nanocrystals embedded in a SiO_2 matrix. Chem Phys Lett 339:319–322
35. Tan C, Wu XL, Deng SS, Huang GS, Liu XN, Bao XM (2003) Blue emission from silicon-based β-SiC films. Phys Lett A 310:236–240
36. Cheng Q, Xu S, Long J, Ostrikov K (2007) Deterministic plasma-aided synthesis of high-quality nanoislanded nc-SiC films. Appl Phys Lett 90:173112